RESEARCH ARTICLE | JULY 30 2025

Scaling strategies for Brinkman penalization in fluid topology optimization

G. Boscolo ; S. Lanzoni ; P. Peruzzo

Physics of Fluids 37, 073645 (2025)
https://doi.org/10.1063/5.0280584

Physics of Fluids ARTICLE pubs.aip.org/aip/pof

Scaling strategies for Brinkman penalization in fluid topology optimization

Cite as: Phys. Fluids **37**, 073645 (2025); doi: 10.1063/5.0280584
Submitted: 13 May 2025 · Accepted: 18 June 2025 ·
Published Online: 30 July 2025

G. Boscolo,[a] S. Lanzoni,[b] and P. Peruzzo[c]

AFFILIATIONS

Department of Civil, Environmental and Architectural Engineering, University of Padova, Padua, Italy

[a]Also at: Polytechnic University of Catalonia, Spain. **Author to whom correspondence should be addressed:** gianmarco.boscolo@phd.unipd.it
[b]**Electronic mail:** stefano.lanzoni@unipd.it
[c]**Electronic mail:** paolo.peruzzo@dicea.unipd.it

ABSTRACT

Topology optimization provides a rigorous framework for determining optimal flow-path designs in fluid mechanics. A popular technique is the density-based approach, which treats fluid–solid interfaces by considering the solid phase as a porous medium with low permeability. Mathematically, such a problem is governed by the Navier–Stokes equations combined with the Brinkman penalization. To consistently solve the optimization problem, this study examines the theoretical foundations of the method, focusing on dimensionless parameters such as the Reynolds number and a specific Darcy number, Da^*. Through dimensional analysis, we derive scaling guidelines for the Brinkman penalization in relation to fluid properties and domain geometry. Numerical simulations show that incorrect scaling can yield nonphysical results, including excessive fluid penetration into solid regions, undermining the optimization. Our findings demonstrate that the invariance of the solution can be maintained by appropriately scaling Da^* with the relative velocity in the porous region, ensuring accurate and reliable results in different scenarios. This work provides a systematic framework for parameter selection in fluid topology optimization, addressing key modeling and computational challenges. By emphasizing the importance of dimensional analysis, it contributes to a broader understanding of topology optimization, paving the way for its more robust and consistent application in fluid mechanics.

I. INTRODUCTION

Several applications in fluid mechanics require the optimal design of flow paths or, more broadly, fluid domains. In recent years, methodological advances and increased computational power have significantly expanded the scope of optimization techniques, reshaping engineering design across a wide range of fluid-related fields. These include aerospace engineering, biomedical applications, and even modeling biological systems and naturally occurring optimization processes.[1] In some cases, optimization involves modifying a preexisting geometric shape.[2] However, in other cases, the solution is not constrained by the initial configuration and requires significant modifications to the initial domain. In such situations, topology optimization plays a crucial role in determining the optimal distribution of fluid–solid phases within the domain. This problem involves two key aspects: (i) the physical-mathematical formulation of the governing equations and (ii) the numerical solution, which relies on different techniques to evolve the topology of the initial domain.[3] One of the most widely used approaches is density-based topology optimization, originally introduced by Bendsøe and Kikuchi.[4] This method solves the Navier–Stokes equations with Brinkman penalization, as proposed in the seminal works of Borrvall and Petersson,[5] Gersborg-Hansen *et al.*,[6] and Olesen *et al.*[7]

In this framework, the fluid domain is partitioned as $\Omega = \Omega_F \cup \Omega_S$, where Ω_F denotes the fluid phase and Ω_S the solid phase, modeled as a porous medium with low permeability. This approach offers a physics-based perspective for solving optimization problems. However, the accuracy of the results strongly depends on the appropriate choice of model parameters, particularly the solid-phase permeability.[8] On the one hand, sufficiently low permeability is needed to represent solid regions accurately; on the other hand, excessively low values can cause numerical instabilities and slow convergence. Striking a balance between these effects is essential for reliable and efficient computations.

The awareness of this issue is steadily growing in the literature and initial attempts to address it have begun to emerge,[8,9] suggesting a gradual maturation of the topic. However, a systematic solution is still lacking. As noted by Alexandersen and Andreasen,[10] the application of topology optimization in fluid mechanics remains largely confined to idealized configurations. Even fewer studies have investigated the transport of solutes or heat convection under realistic conditions.[11,12] In such cases, the model parameters are often chosen empirically and without a clear physics-based rationale. This empirical approach limits the predictive power of optimization results and their applicability to complex engineering problems. In particular, the physics-based selection of permeability values in the solid phase continues to represent a major obstacle to the wider adoption of topology optimization in fluid systems, in contrast to its success in solid mechanics.

A physically consistent selection of porous-medium parameters would significantly enhance the robustness and reliability of optimized designs. In biomedical engineering, for instance, it could support the development of patient-specific stent grafts by building on the foundational work of Quarteroni and Rozza[13] and capturing realistic blood flow features under pathological conditions.[14] In microfluidics, it would allow the design of more efficient chemical reactors,[15] Venturi diodes,[16] and microfluidic mixers and separators[17] such as microfluidic chips.[18] Similarly, in thermal management, it would strengthen the design of high-performance heat sinks and heat exchangers.[19] These examples illustrate the importance of advancing topology optimization modeling practices to achieve advanced high-performance fluid systems in diverse industries.

This study aims to clarify the role of modeling parameters in the density-based formulation by analyzing flow behavior in both fluid and porous regions, following a methodology akin to the numerical approach introduced by Guest and Prévost.[20] We first identify the key dimensionless groups that govern the optimization problem, namely, the characteristic Reynolds and Darcy numbers, and then validate the proposed formulation through numerical simulations. Based on these results, we propose criteria to reinforce the density-based method, focusing on the consistency of the optimal solution and its sensitivity to the computational mesh resolution.

II. DEFINITION OF THE DENSITY-BASED APPROACH

The partial differential equations (PDEs) governing the flow in a domain composed of a fluid bounded by a solid phase, treated as a medium with small permeability, are the Navier–Stokes equations with Brinkman penalization, namely,

$$\rho \frac{d\mathbf{u}}{dt} - \mu \nabla^2 \mathbf{u} + \nabla p = -\alpha(\gamma)\mathbf{u}, \tag{1a}$$

$$\nabla \cdot \mathbf{u} = 0, \tag{1b}$$

where ρ and μ are the density and viscosity of the fluid, respectively, while $\alpha(\gamma)$ is the Brinkman penalization term, which depends on the domain indicator function $\gamma(\mathbf{x})$ and accounts for the flow resistance within the porous medium surrounding the fluid. The latter function, which identifies the points belonging to the solid domain Ω_S, and thus the Brinkman penalization term, read

$$\gamma(\mathbf{x}) = \begin{cases} 0 & \mathbf{x} \in \Omega_F \\ 1 & \mathbf{x} \in \Omega_S \end{cases}, \quad \alpha(\gamma(\mathbf{x})) = \begin{cases} \alpha_{min} \approx 0 & \mathbf{x} \in \Omega_F, \\ \alpha_{max} \gg 1 & \mathbf{x} \in \Omega_S, \end{cases} \tag{2}$$

with α_{min} and α_{max} denote the lower and upper bounds of the flow resistance, respectively.

The topology optimization problem consists of minimizing the fluid energy dissipation under a maximum fluid volume constraint. It can be formulated as follows:

$$\begin{cases} \min_\gamma J(\mathbf{u},\gamma) = & \int_\Omega \alpha(\gamma)|\mathbf{u}|^2 d\Omega + \frac{1}{2}\mu \int_\Omega |\nabla \mathbf{u} + \nabla \mathbf{u}^T|^2 d\Omega, \\ \text{subject to:} & \\ & |\Omega_F| \leq V_r \cdot |\Omega|, \\ & \gamma(\mathbf{x}) \in \{0,1\} \forall \mathbf{x} \in \Omega, \end{cases} \tag{3}$$

where $\mathbf{u}$ satisfies the governing equations (1), $J(\mathbf{u},\gamma)$ is the objective functional, and V_r is the target volume to be occupied by the fluid phase. The operator $|\cdot|$ indicates the Euclidean norm when applied to vectors, the Frobenius norm when applied to matrices, and the volume when applied to Ω, Ω_F or Ω_S.

The numerical treatment of the topology optimization problem Eq. (3) is iterative with each step consisting of solving the governing equations followed by an update of the distribution of γ based on the objective functional and its derivatives. In this numerical context, the fluid and solid phases are typically modeled assuming $\gamma(\mathbf{x}) \in [0,1]$ continuous across the domain, Ω, with the corresponding penalization factor defined as the convex function

$$\alpha(\gamma) = \alpha_{min} + (\alpha_{max} - \alpha_{min}) \frac{\varphi\gamma}{\varphi + 1 - \gamma}, \tag{4}$$

where the parameter φ controls the sharpness of the numerical approximation of Eq. (2). As demonstrated by Borrvall and Petersson[5] and Olesen *et al.*,[7] this formulation ensures an optimal solution that automatically partitions the domain into Ω_F and Ω_S with a continuous formulation of $\gamma(\mathbf{x})$ that mimics a smoothed Heaviside function.[21,22]

III. THE MISINTERPRETATION OF THE BRINKMAN PENALIZATION FACTOR

The penalization factor, α, governs the optimal design of flow paths within a fluid domain bounded by a modifiable solid phase, aiming to minimize the expenditure of fluid energy while respecting a maximum volume of fluid. More precisely, the penalization factor can be expressed as $\alpha = \mu/k$, where k is the permeability of the porous medium surrogating the solid phase. Although this relation is standard in groundwater flows, issues arise when the Brinkman model is used in topology optimization. In Ref. 5, α is described as an "inverse permeability," seemingly neglecting the role of fluid viscosity. However, their formulation consistently scales α with μ. Despite this, interpreting α as an inverse permeability remains common in the literature with some exceptions (e.g., Okkels *et al.*,[23] Shin *et al.*,[24] Jensen[25]). While the interpretation of the penalization factor as the inverse of permeability is valid when the fluid viscosity remains constant, it can lead to erroneous optimal flow-path shapes in cases where the analysis is applied to systems involving fluids with different properties (viz., density and viscosity).

This aspect is illustrated in Fig. 1, which considers a rectangular two-dimensional (2D) domain of height $H = 6\,\text{cm}$ and length $L = 9\,\text{cm}$ with two inlets and two outlets on opposite sides of width $D = 1\,\text{cm}$ [Fig. 1(a)]. A parabolic inflow profile with peak velocity $U_M = 1.5\,\text{cm/s}$ is prescribed at both inlets, while zero pressure is imposed at the outlets. The optimal channel layout is tested using three different fluids, all with the same maximum penalization

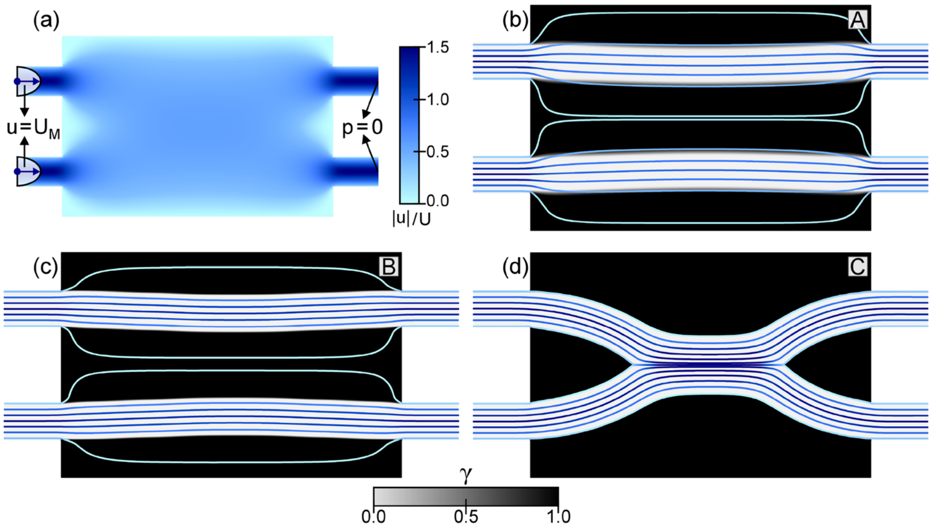

FIG. 1. Optimal solution for three double-inlet-outlet case studies reported in Table I. (a) Boundary conditions and velocity field ($Re = 1$) at the first iteration, when $\Omega_F = \Omega$. (b)–(d) Results of the topology optimization obtained for $V_r = 0.334$, $\varphi = 0.1$, and $\alpha_{max} = 10^3$ Pa · s/m^2 after 300 iterations for cases A, B, and C, respectively. Streamlines originating from the inlets are also shown, colored according to the relative velocity magnitude.

$\alpha_{max} = 10^3\ \mathrm{Pa \cdot s/m^2}$ and a fixed Reynolds number $Re = \rho U D/\mu = 1$, where U is the average inlet velocity (see Table I).

Neglecting the effect of a change in viscosity alters the fluid motion within the porous medium. In cases A and B, the optimal design features two nearly straight channels [Figs. 1(b) and 1(c)], unlike case C, which yields a central channel with a confluence from the inlets and a bifurcation toward the outlets [Fig. 1(d)]. A similar configuration is also observed by Guest and Prévost,[20] although it was obtained using a different set of parameters. The present example highlights the importance of adopting a physics-based criterion for setting the Brinkman penalization, as proposed through dimensional analysis in Sec. IV.

IV. DIMENSIONAL ANALYSIS OF THE BRINKMAN EQUATION FOR FLUID TOPOLOGY OPTIMIZATION

The dimensional analysis of the optimization problem is made by introducing the characteristic length scale, ℓ_0, and the velocity scale, u_0, to properly weight the various terms in Eq. (1a). These scales attain significantly different values in the fluid and porous phases. In the fluid region, the hydrodynamic scales are determined by the characteristic width D and velocity U of the channelized patterns (i.e., $\ell_0 = D$ and $u_0 = U$). In the fluid domain, Ω_F, the dimensionless form of Eq. (1a) thus becomes

$$\frac{d\tilde{\mathbf{u}}}{d\tilde{t}} - \frac{1}{Re}\tilde{\nabla}^2\tilde{\mathbf{u}} + \tilde{\nabla}\tilde{p} = -\frac{a_{min}D^2}{\mu}\frac{1}{Re}\tilde{\mathbf{u}} = 0, \tag{5}$$

where $\tilde{t} = t\,u_0/\ell_0$, $\tilde{\mathbf{x}} = \mathbf{x}/\ell_0$, $\tilde{\mathbf{u}} = \mathbf{u}/u_0$, $\tilde{p} = p/(\rho\, u_0^2)$, and $a_{min} \to 0$. However, in the region occupied by the porous medium, the flow described by the Brinkman approach occurs through irregular micro channels whose size d is determined by the pores of the medium. The velocity within these channels is represented through an equivalent filtration velocity, V, defined as

$$V = \lim_{\delta\lambda \to 0} \frac{\delta q}{\delta \lambda}, \tag{6}$$

with δq being the specific flow rate through a small segment of length $\delta\lambda$. Due to the small spatial scale d, the flow in the Ω_S region is expected to be dominated by viscosity. Setting $\ell_0 = d$, $u_0 = V$, and scaling the pressure as $p \propto \mu V/d$, the dimensionless form of Eq. (1a) reads

$$\frac{d\tilde{\mathbf{u}}}{d\tilde{t}} - \frac{1}{Re_S}\tilde{\nabla}^2\tilde{\mathbf{u}} + \frac{1}{Re_S}\tilde{\nabla}\tilde{p} = -\frac{\alpha_{max}\,d^2}{\mu}\frac{1}{Re_S}\tilde{\mathbf{u}}, \tag{7}$$

where $Re_S = \rho\,Vd/\mu$ is the characteristic Reynolds number in Ω_S.

The ratios of the scaling variables establish the connection between the subdomains Ω_F and Ω_S. Specifically, we introduce the velocity ratio, $r_u = V/U$, which links the characteristic velocities of the two subdomains, and the size ratio, $r_\ell = d/D$, which relates the characteristic lengths. These scaling ratios parameters are critical to consistently model the dynamics within the fluid and the porous regions. In particular, Re_S depends on Re through the relation $Re_S = r_\ell\, r_u\, Re$.

In the present application of hydrodynamic optimization, both the velocity and size ratios are assumed to be small enough to ensure that $Re_S \ll 1$ and, consequently, the flow in Ω_S is of creeping type. Equation (7) can thus be simplified as

$$\tilde{\nabla}^2\tilde{\mathbf{u}} + \tilde{\nabla}\tilde{p} = -\frac{1}{Da}\tilde{\mathbf{u}}, \tag{8}$$

where $Da = k_{min}/d^2$ is the Darcy number, $k_{min} = \mu/\alpha_{max}$ being the lowest value of the permeability. The Darcy number is thus the key parameter that controls the fluid dynamics in Ω_S. In addition, ensuring the invariance of the topology optimization solution requires maintaining constant ratios between the terms that makeup the objective

TABLE I. Physical parameters for the considered three test cases.

	ρ (kg/m^3)	μ (Pa s)	U (m/s)	D (m)	Re
Case A	10	10^{-3}	0.01	0.01	1
Case B	1	10^{-4}	0.01	0.01	1
Case C	0.1	10^{-5}	0.01	0.01	1

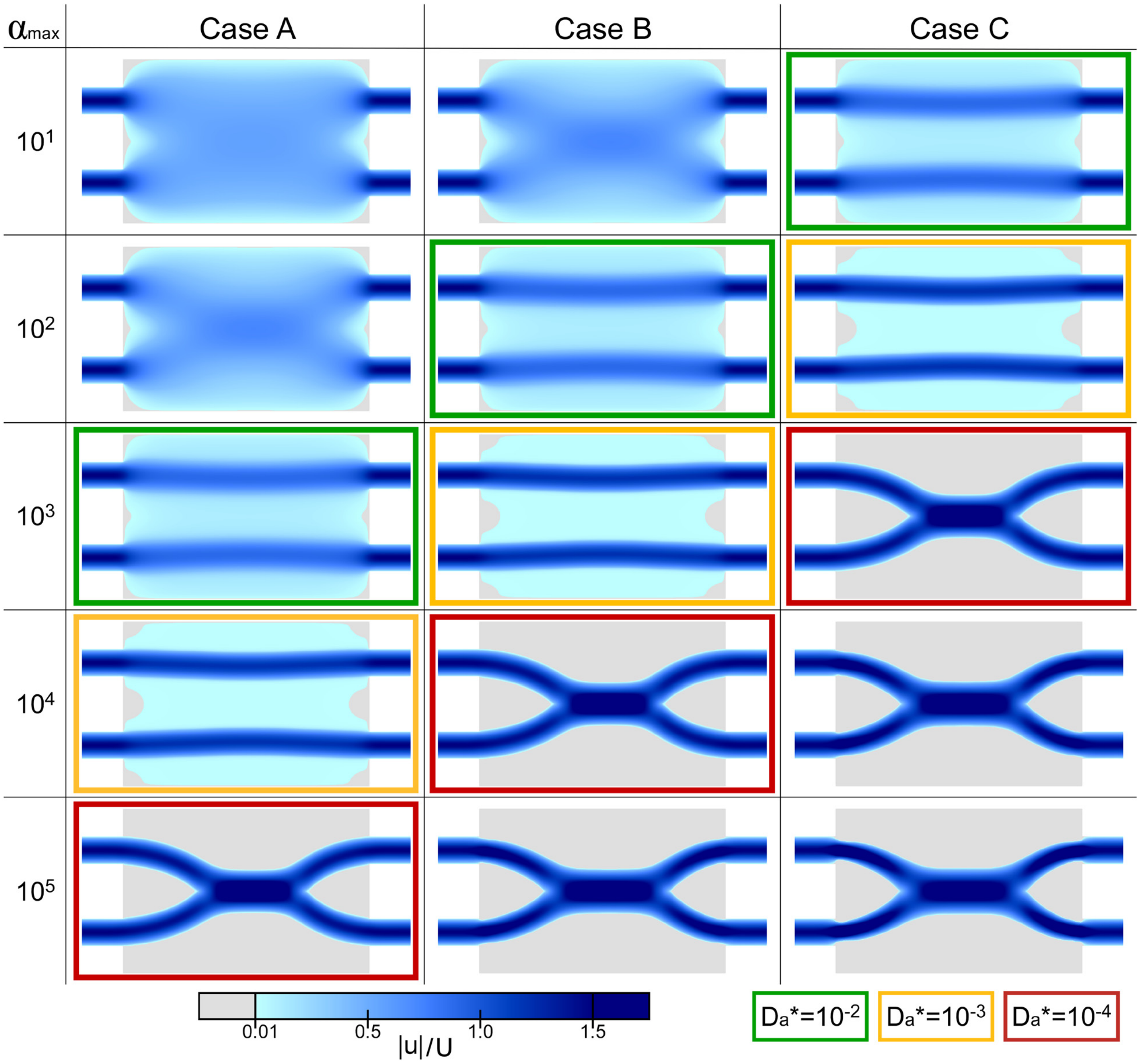

FIG. 2. Dimensionless velocity field, $|\mathbf{u}|/U$, after 300 iterations for the case studies reported in Table I, obtained by varying α_{max} from 10^1 to 10^5 Pa s/m^2. Colored frames indicate the value of Da^* equal to 10^{-2} (green), 10^{-3} (yellow), and 10^{-4} (red), whose optimal design parameter distribution is reported in Fig. 1, for the three analyzed scenarios.

functional J. In the considered formulation [see Eq. (3)], the functional consists of the Brinkman penalization term, J_α, and the viscous dissipation term, $J_{\nabla u}$, which scale as

$$J_\alpha = \int_\Omega \alpha(\gamma)\,|\mathbf{u}|^2\, d\Omega \propto \alpha_{max}\, V^2, \tag{9a}$$

$$J_{\nabla u} = \frac{1}{2}\mu \int_\Omega |\nabla\mathbf{u} + (\nabla\mathbf{u})^T|^2\, d\Omega \propto \frac{\mu\, U^2}{D^2}, \tag{9b}$$

$$r_J = \frac{J_{\nabla u}}{J_\alpha} \propto \frac{r_\ell^2}{r_u^2}\, Da. \tag{9c}$$

It follows that $r_u \propto (Da^*/r_J)^{1/2}$, with $Da^* = r_\ell^2\, Da$ a modified Darcy number. Using the definitions of r_ℓ and Da then results

$$Da^* = \frac{\kappa_{min}}{D^2} = \frac{\mu}{\alpha_{max}\, D^2}. \tag{10}$$

We observe that, in solutions where the solid phase is accurately modeled by insertion of the porous medium (i.e., with negligible velocities), the dissipative contribution associated with the Brinkman term is typically small compared to the viscous dissipation within the fluid.[26] As a result, it is reasonable to assume $r_J \geq 1$, indicating that $\sqrt{Da^*}$ provides an upper bound for r_u.

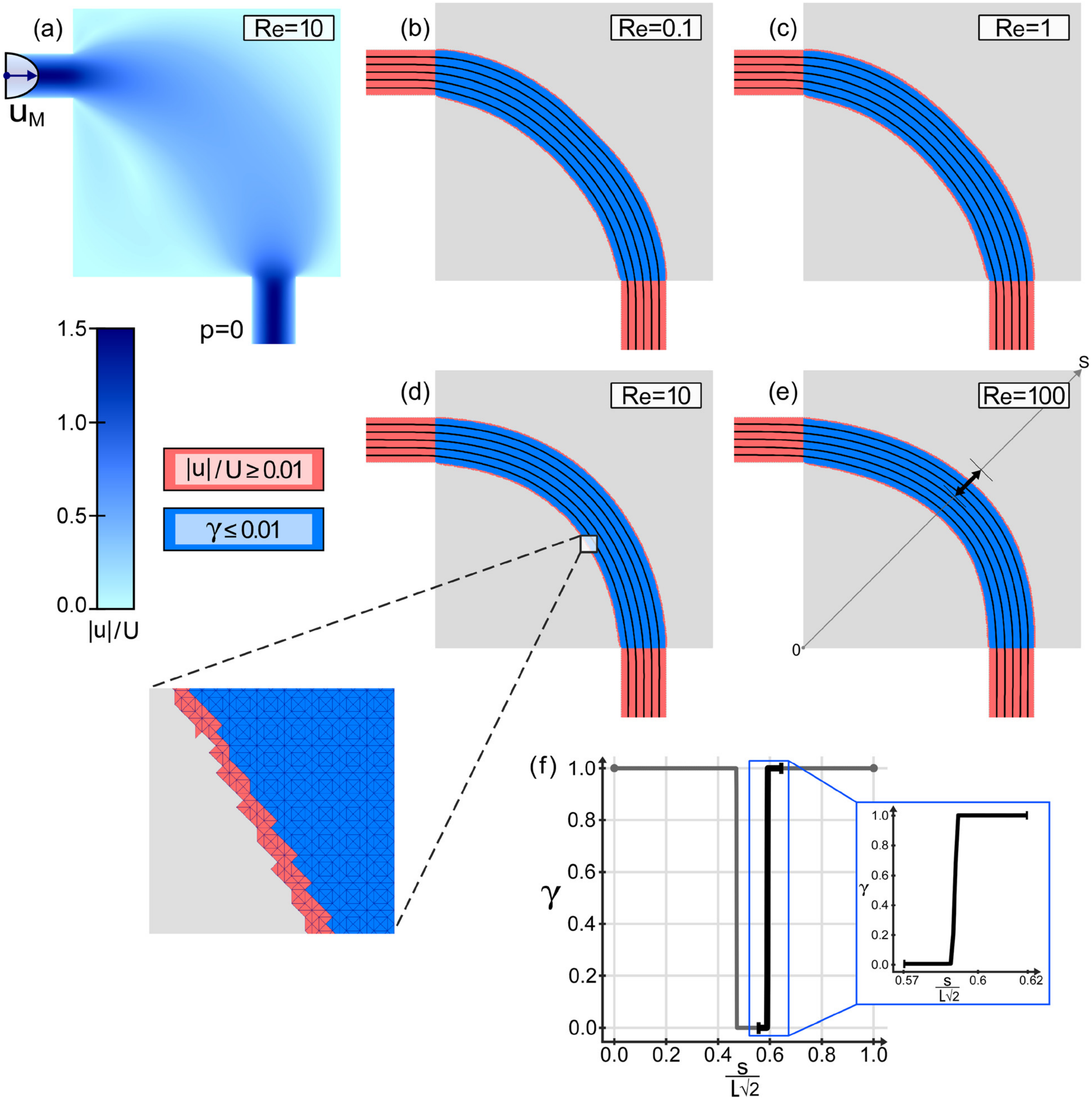

FIG. 3. Optimal solutions for the pipe-bend problem with $V_r = 0.2$, $\varphi = 0.1$, and initial condition $\Omega_F = \Omega$. (a) Boundary conditions and velocity field at the first iteration for $Re = 10$. (b)–(e) Superposition of regions with $|\mathbf{u}|/U \geq 0.01$ (red) and optimal geometries ($\gamma \leq 0.01$, in blue) after 200 iterations. Streamlines originating from the inlet are also shown. Results are provided for $Re = 0.1$–100 and a constant value of $Da^* = 10^{-4}$. (f) Distribution of the design variable, γ, along the diagonal line shown in panel (e), parametrized by s, for $Re = 100$. The thicker portion corresponds to the fluid–solid interface, highlighted in black. The inset shows a zoom of this region.

The solution to the dimensionless optimization problem eventually depends on three parameters: Re, Da, and Da^*. Since, by definition, Da and Da^* are related together through the square of the length ratio, r_ℓ is an implicit parameter ensuring that the invariance of Re and Da^* is a necessary and sufficient condition for obtaining a particular optimal solution. Note that both Re and Da^* are defined in terms of the characteristic scales of the fluid domain, which are the only ones that need to be explicitly prescribed in the problem formulation Eq. (3). The same relationship between α and the current definition of Da^* has recently been proposed in the literature.[27–29] In those studies, the criterion was derived through dimensional analysis, assuming the same characteristic length and velocity scales in both the fluid and

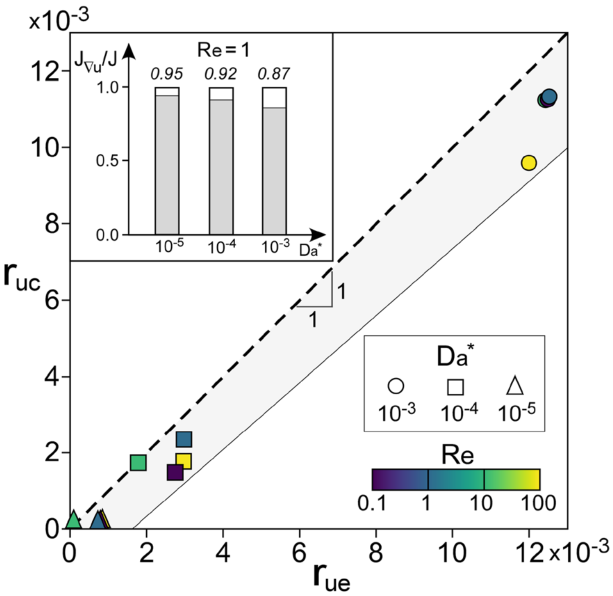

FIG. 4. Comparison between the theoretical and computed values of the velocity scales ratio, respectively r_{ue} and r_{uc}, for different Reynolds numbers ($Re = 0.1$, 1, 10, 100) and modified Darcy numbers ($Da^* = 10^{-3}, 10^{-4}, 10^{-5}$) in the pipe-bend problem. The bar chart represents the percentage of the objective functional associated with viscous dissipation.

solid regions. As a result, Da^* appears directly in the governing equation, while, in the present work, it emerges from the invariance of the objective function. Therefore, according to our analysis, different definitions of Da^* may arise depending on the specific functional J used in the problem.

A. Estimate of the fluid–solid interface thickness

Coupled modeling of fluid-porous media using Darcy's equations typically leads to a velocity discontinuity at the interface.[30] In contrast, the Brinkman penalization approach ensures a smooth velocity transition between Ω_F and Ω_F.[31] Although this continuity is beneficial for modeling free-flow/porous-medium interfaces,[32] it poses a limitation in density-based topology optimization, where the porous medium is used to surrogate the solid phase.

As a first approximation, the length scale of this transition zone, δ, has been defined by Neale and Nader[31] considering a one-dimensional parallel flow in a channel with a permeable wall. The closed form solution of this problem shows that the velocity module decay exponentially from the mean channel flow velocity U to the limiting value V in the porous region. This latter limiting value reads

$$V \simeq 3U\left(\frac{2(1+\sigma)}{1+(1+\sigma)^2}\right)^2, \tag{11}$$

with $\sigma = 1/\sqrt{Da^*}$ (see Subsection 1 of Appendix A for details).

For density-based topology optimization purposes, the transition zone can be identified as the layer in which the velocity decreases from $|\mathbf{u}| \sim U$ to $|\mathbf{u}| \sim V_\delta = r_{V_\delta} U$, with r_{V_δ} being the sufficiently small ratio between the velocity at the fluid–solid interface and the characteristic velocity in the fluid domain. In this context, although the transition layer thickness formula by Neale and Nader[31] was originally expressed in terms of a multiple of V, here δ is instead expressed in terms of a fraction of U (i.e., r_{V_δ}), leading to (see Subsection 2 of Appendix A for details)

$$\frac{\delta}{D} = -\frac{1}{\sigma}\ln\left\{\frac{2(1+\sigma)}{\sigma^2-2}\left[\frac{r_{V_\delta}}{3}\left(\frac{1+(1+\sigma)^2}{2(1+\sigma)}\right)^2 - 1\right]\right\}. \tag{12}$$

Within the transition region, the velocity is higher than V_δ, therefore, $\alpha(\gamma)$ will be slightly lower than α_{max} (i.e., $\gamma \lesssim 1$) to counteract the increase in dissipation in the porous medium.

Consequently, appropriately treating the fluid–solid interface is crucial and requires choosing the characteristic mesh size, h, to ensure that at least one element lies within the transition zone, i.e., $h \le \delta$. According to the relation linking r_u and Da^*, setting $r_{V_\delta} = \sqrt{Da^*}$ in Eq. (12) could be a reasonable criterion to determine h. Since it must hold that $r_u \le r_{V_\delta}$, to obtain a velocity in the porous medium at least two orders of magnitude smaller than U, as proposed by Alexandersen,[26] it can be chosen $Da^* \le 10^{-4}$.

V. NUMERICAL ASSESSMENT OF THEORETICAL PREDICTIONS

We assessed the validity of the dimensional analysis by comparing the results of the three case studies in Table I, varying the parameter α_{max}. The governing equations (1) were solved numerically using the finite element method (FEM). The domain was discretized with a triangular mesh, totalling 384 000 elements. Functional derivatives with respect to γ were computed using the continuous adjoint method.[33] The domain design was iteratively updated via the method of moving asymptotes (MMA, Svanberg[34]) with convergence defined by a relative change of the design parameter γ below 10^{-5}. Figure 2 shows the velocity magnitude in regions where it exceeds 1% of the mean inlet velocity, U. Unlike the design parameter distribution—which yields an optimal geometry similar to those in Fig. 1 (see Fig. 5 in Appendix B)—the velocity field analysis offers an additional, physically meaningful criterion for evaluating the correctness of the solution. Too low values of α_{max} (i.e., too high Da^*) result in a fluid–solid interface that remains permeable, producing a heterogeneous velocity field with proto-channels and extended regions of low but non-zero velocity (see cases A and B with $\alpha_{max} = 10^2$ and 10^1 Pa $\cdot$ s/m^2, respectively, in Fig. 2). Although physically consistent, these results poorly represent optimal flow topologies. As α_{max} increases, the interface sharpens. In accordance with the dimensional analysis, identical values of Da^* produce the same optimal configurations in the various cases (Fig. 2). This confirms also the findings of Abdelhamid and Czekanski[9] about the density-independence of Brinkman penalization at low Re. The values of $Da^* \le 10^{-3}$ (yellow/red box in Fig. 2) sufficiently slow the flow in Ω_S, allowing well-defined channels to form in Ω_F. In particular, $Da^* = 10^{-4}$ (red boxes) yields near-optimal geometries with filtration velocity in Ω_S approximately two orders of magnitude lower than in Ω_F, consistent with $r_u \lesssim \sqrt{Da^*}$ and the results from Kreissl *et al.*,[35] However, values of $Da^* \le 10^{-6}$ may lead to non-convergent solutions due to numerical instabilities.[36]

To illustrate in detail the behavior of the fluid–solid interface obtained by using the strategy discussed in Sec. IV A, we considered the "pipe-bend" problem. In this application, we investigated a square domain of side $L = 6\,\mathrm{cm}$ with an inlet and an outlet of width $D = 1\,\mathrm{cm}$ located near the beginning and the end of two adjacent sides [Fig. 3(a)]. Optimal configurations and non-negligible velocity regions are shown in Figs. 3(b) and 3(e) for Re from 10^{-1} to 10^{2} and a fixed value of $Da^* = 10^{-4}$. The computational mesh size has been chosen according to Eq. (12) with $r_{V_\delta} = \sqrt{Da^*} = 10^{-2}$.

The results show that while the channel bend curvature increases with Re, the thickness of the interface remains constant, covering about 1–2 elements [see inset in panel (d)] and a small portion of the domain size (Fig. 3). This finding confirms the validity of the estimate for the thickness of the fluid–solid interface provided by Eq. (12). The reliability of the filtration velocity estimate is assessed by comparing the theoretical estimate of r_u obtained from the relation (9c), i.e., setting $r_{ue} = (Da^*/r_J)^{1/2}$, with the average numerical value of the velocity scale ratio across $\Omega_S^{opt} = \{\mathbf{x}|\gamma(\mathbf{x}) > 0.01\}$

$$r_{uc} = \frac{1}{|\Omega_S^{opt}|}\left(\int_{\Omega_S^{opt}} |\frac{u}{U}|^2 d\Omega\right)^{1/2}. \tag{13}$$

The relationship between r_{ue} and r_{uc} is illustrated in Fig. 4 for the pipe-bend problem, with Da^* now also varying from 10^{-5} to 10^{-3}. The representative points fall below the perfect alignment line, suggesting that the theoretically estimated values (r_{ue}) tend to slightly overestimate the average velocity numerically computed in Ω_S^{opt}. In addition, these latter points are organized almost parallel to the diagonal, indicating a linear dependence between r_u and $(Da^*/r_J)^{1/2}$. The clustering of points with identical Da^* further supports the theoretical prediction that the Reynolds number in the fluid domain (at least for the laminar conditions here considered) has little influence on the velocity within the porous medium, as experimentally demonstrated by Choi and Waller[37] and Goharzadeh *et al.*[38] The histogram in the inset of Fig. 4 shows the percentage of objective functional associated with viscous dissipation, $J_{\nabla u}/J$. As Da^* decreases, the solid phase is represented more accurately and the thickness of the fluid–solid interface is reduced. Consequently, the percentage of objective functional related to the Brinkman penalization, J_α/J, decreases, leading to a functional evaluation that more closely approximates the actual value in the optimal geometry.

VI. CONCLUSIONS

In this work, we have formulated and analyzed the dimensionless parameters that govern the behavior of the Navier–Stokes–Brinkman equation, commonly implemented in density-based schemes for topology optimization problems in domains with fluid–solid interfaces. We have demonstrated that the invariance of the optimal solution generally depends on the Reynolds number, Re, and on a modified Darcy number, Da^*. The latter parameter controls the dissipation within the porous media—used to represent the solid region—and the transition at its interface with the fluid domain. Our analysis shows that the ratio between the limiting velocity in the porous region, V, and the characteristic velocity of the fluid domain, U, is upper-bounded by a linear function of $\sqrt{Da^*}$. This relation allows for a proper selection of the mesh size in the interface region by means of Eq. (12), setting $r_{V_\delta} = \sqrt{Da^*} = 10^{-2}$. Since Da^* mirrors the penalization parameter α, these findings have significant implications for configuring density-based models in fluid dynamics beyond the standard cases studied in the literature. This could encourage broader adoption of the technique in real-world applications.

ACKNOWLEDGMENTS

The authors thank Andrea Gorgi for his contribution to the development of the code used in this work.

AUTHOR DECLARATIONS

Conflict of Interest

The authors have no conflicts to disclose.

Author Contributions

G. Boscolo: Conceptualization (equal); Formal analysis (equal); Investigation (equal); Methodology (equal); Software (lead); Validation (equal); Visualization (lead); Writing – original draft (lead). **S. Lanzoni:** Conceptualization (supporting); Formal analysis (equal); Investigation (supporting); Methodology (equal); Supervision (equal); Validation (supporting); Visualization (supporting); Writing – review & editing (equal). **P. Peruzzo:** Conceptualization (equal); Formal analysis (equal); Investigation (equal); Methodology (equal); Supervision (equal); Validation (equal); Visualization (supporting); Writing – original draft (supporting); Writing – review & editing (equal).

DATA AVAILABILITY

The data that support the findings of this study are openly available in github at https://github.com/GianmarcoBoscolo/FTOPT, Ref. 39.

APPENDIX A: FLUID–SOLID INTERFACE THICKNESS

1. Evaluation of the limiting velocity in the porous media

According to Neale and Nader,[31] the closed formula for the velocity profile of a steady, incompressible laminar flow through a two-dimensional parallel channel bounded by a porous medium, governed by the Navier–Stokes equations with Brinkman penalization, is

$$\mathbf{u}_\sigma(\lambda) = \begin{cases} \mathbf{u}_\sigma^F(\lambda) = V_\sigma^\infty \cdot [c + b\lambda + a\lambda^2] & \lambda \in [0,1], \\ \mathbf{u}_\sigma^P(\lambda) = V_\sigma^\infty \cdot \left[1 + \frac{b}{\sigma} e^{\lambda\sigma}\right] & \lambda \in [-\infty, 0], \end{cases} \tag{A1}$$

where λ is the transversal direction ($\lambda \in [0,1]$ means pure fluid domain, $\lambda \in [-\infty, 0]$ means porous domain), $\sigma = 1/\sqrt{Da^*}$, V_σ^∞ is the limiting porous media velocity and a, b, c are defined as

$$\begin{aligned} a &= -\frac{1}{2}\sigma^2, \\ b &= \frac{\sigma^2 - 2}{2(1+\sigma)}\sigma, \\ c &= \frac{\sigma(\sigma+2)}{2(1+\sigma)} = b \cdot \frac{\sigma+2}{\sigma^2-2}. \end{aligned} \tag{A2}$$

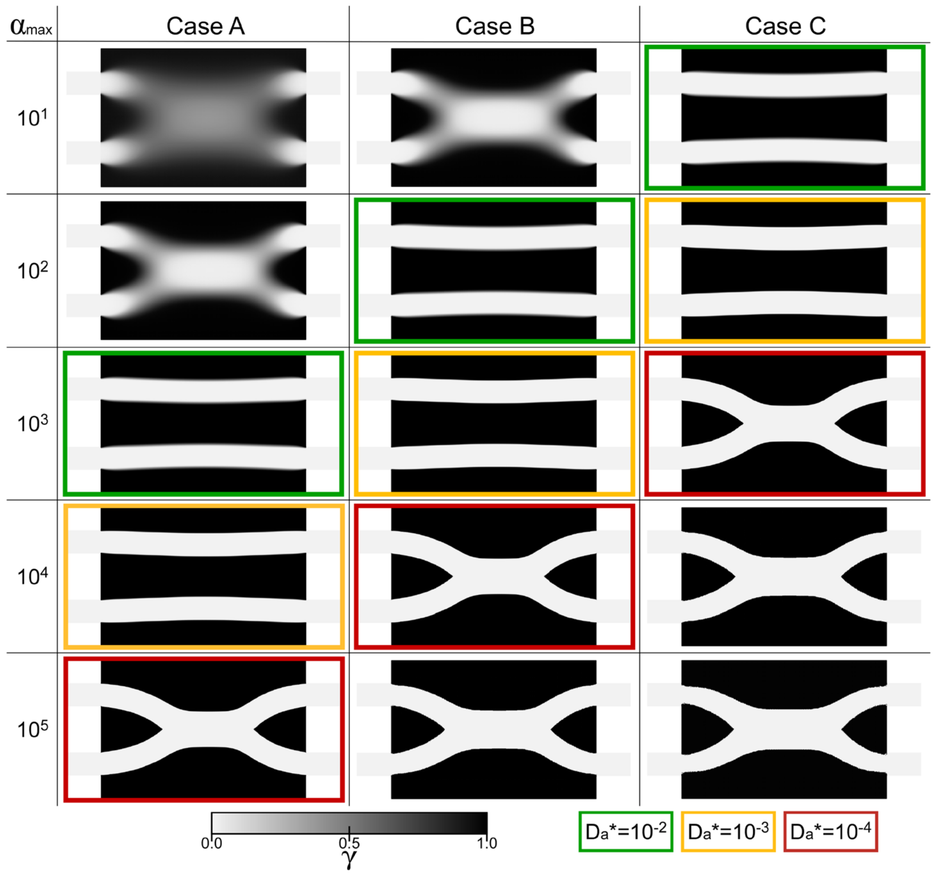

FIG. 5. Distribution of the design parameter γ after 300 iterations for the case studies reported in Fig. 2, obtained by varying α_{max} from 10^1 to 10^5 Pa s/m^2. Colored frames indicate the value of Da^* equal to 10^{-2} (green), 10^{-3} (yellow), and 10^{-4} (red) for the three analyzed scenarios.

For the sake of applying them to density-based topology optimization analysis, the velocity profile should be rewritten in terms of U and not V_σ^∞. Exploiting the parabolic profile of the velocity in the fluid phase its maximum value reads

$$\begin{aligned}\mathbf{u}^F_{\sigma_{max}} &= V_\sigma^\infty \cdot \left[c - \frac{b^2}{4a}\right] = V_\sigma^\infty \cdot b\left[\frac{\sigma+2}{\sigma^2-2} + \frac{\sigma^2-2}{4\sigma(1+\sigma)}\right]\\ &= V_\sigma^\infty \cdot \left[\frac{\sigma^4+4\sigma^3+8\sigma^2+8\sigma+4}{8(1+\sigma)^2}\right]\\ &= \frac{V_\sigma^\infty}{2} \cdot \left[\frac{1+(1+\sigma)^2}{2(1+\sigma)}\right]^2.\end{aligned}$$

Since the average velocity in the fluid phase can be expressed as $U_\sigma = \frac{2}{3}\mathbf{u}^F_{\sigma_{max}}$, it holds

$$U_\sigma = \frac{V_\sigma^\infty}{3} \cdot \left[\frac{1+(1+\sigma)^2}{2(1+\sigma)}\right]^2,$$

that finally leads to

$$V_\sigma^\infty = 3U_\sigma \cdot \left[\frac{2(1+\sigma)}{1+(1+\sigma)^2}\right]^2, \tag{A3}$$

that is Eq. (11). It can also be observed that the limiting velocity scales ratio reads

$$r_\sigma^\infty = \frac{V_\sigma^\infty}{U_\sigma} = 3 \cdot \left[\frac{2(1+\sigma)}{1+(1+\sigma)^2}\right]^2.$$

2. Evaluation of the transition zone thickness

The ratio of the velocity with respect to U_σ is defined as

$$r_\sigma(\lambda) = \mathbf{u}_\sigma(\lambda)/U_\sigma.$$

Substituting Eq. (A3) in Eq. (A1) yields

$$r_\sigma(\lambda) = \begin{cases} r_\sigma^F(\lambda) = r_\sigma^\infty \cdot [c + b\lambda + a\lambda^2] & \lambda \in [0,1],\\ r_\sigma^P(\lambda) = r_\sigma^\infty \cdot \left[1 + \frac{b}{\sigma}\exp(\lambda\sigma)\right] & \lambda \in [-\infty, 0[.\end{cases}$$

Therefore, chosen an acceptable velocity ratio in the porous phase $\bar{r} \in]r_\sigma^\infty, r_\sigma(0)[$, the value of λ in which this is attained can be obtained by inverting the formula for $r_\sigma^P(\lambda) = \bar{r}$, that leads to

$$|\lambda| = -\frac{1}{\sigma}\ln\left\{\frac{2(1+\sigma)}{\sigma^2-2}\left[\frac{\bar{r}}{3}\left(\frac{1+(1+\sigma)^2}{2(1+\sigma)}\right)^2 - 1\right]\right\},$$

that is the formula used to estimate δ/D in Eq. (12) setting $\bar{r} = r_{V_\delta}$.

APPENDIX B: DESIGN PARAMETER PLOT FOR CASE STUDIES OF FIG. 2

Figure 2 illustrates how the velocity field effectively captures the impact of the Brinkman resistance parameter used to model the porous medium. Figure 5 shows the corresponding design variable distribution, γ. The panels with $Da^* = 10^{-2}, 10^{-3}$, and 10^{-4} match the results shown for cases A, B, and C in Fig. 1, respectively. For $Da^* < 10^{-2}$ (i.e., values above the green highlighted panels), the optimization procedure fails to converge to a partitioned domain due to the insufficient resistance at the porous/fluid interface. This results in an inadequate penalization contribution within the cost functional. In contrast, the panels corresponding to $Da^* > 10^{-4}$ reveal the occurrence of numerical instabilities discussed in Sec. V.

REFERENCES

[1]D. Thévenin and G. Janiga, *Optimization and Computational Fluid Dynamics* (Springer Science & Business Media, 2008).
[2]B. Mohammadi and O. Pironneau, *Applied Shape Optimization for Fluids* (OUP, Oxford, 2009).
[3]M. P. Bendsoe and O. Sigmund, *Topology Optimization: Theory, Methods, and Applications* (Springer Science & Business Media, 2013).
[4]M. P. Bendsøe and N. Kikuchi, "Generating optimal topologies in structural design using a homogenization method," Comput. Methods Appl. Mech. Eng. **71**, 197–224 (1988).
[5]T. Borrvall and J. Petersson, "Topology optimization of fluids in stokes flow," Int. J. Numer. Methods Fluids **41**, 77–107 (2003).
[6]A. Gersborg-Hansen, O. Sigmund, and R. B. Haber, "Topology optimization of channel flow problems," Struct. Multidiscip. Optim. **30**, 181–192 (2005).
[7]L. H. Olesen, F. Okkels, and H. Bruus, "A high-level programming-language implementation of topology optimization applied to steady-state Navier–Stokes flow," Int. J. Numer. Methods Eng. **65**, 975–1001 (2006).
[8]M. J. Theulings, M. Langelaar, F. van Keulen, and R. Maas, "Towards improved porous models for solid/fluid topology optimization," Struct. Multidiscip. Optim. **66**, 133 (2023).
[9]M. Abdelhamid and A. Czekanski, "On the calculation of the Brinkman penalization term in density-based topology optimization of fluid-dependent problems," arXiv:2302.14156 (2023).
[10]J. Alexandersen and C. S. Andreasen, "A review of topology optimisation for fluid-based problems," Fluids **5**, 29 (2020).
[11]T. Dbouk, "A review about the engineering design of optimal heat transfer systems using topology optimization," Appl. Therm. Eng. **112**, 841–854 (2017).
[12]L. Li, J. Xu, and S. Li, "Topology optimization of microchannel structures for enhanced heat flow in liquid cooling garments," Phys. Fluids **36**, 127140 (2024).
[13]A. Quarteroni and G. Rozza, "Optimal control and shape optimization of Aorto-Coronaric bypass anastomoses," Math. Models Methods Appl. Sci. **13**, 1801–1823 (2003).
[14]D. H. Alonso and E. C. N. Silva, "Topology optimization for blood flow considering a hemolysis model," Struct. Multidiscip. Optim. **63**, 2101–2123 (2021).
[15]F. Okkels and H. Bruus, "Scaling behavior of optimally structured catalytic microfluidic reactors," Phys. Rev. E **75**, 016301 (2007).
[16]Z. Liu, Y. Deng, S. Lin, and M. Xuan, "Optimization of micro Venturi diode in steady flow at low Reynolds number," Eng. Optim. **44**, 1389–1404 (2012).
[17]Y. Deng, Y. Wu, and Z. Liu, "Topology optimization theory for laminar flow," in *Applications in Inverse Design of Microfluidics* (Springer, 2018).
[18]X. Chen and T. Li, "A novel design for passive misscromixers based on topology optimization method," Biomed. Microdevices **18**, 1–15 (2016).
[19]F. Feppon, G. Allaire, C. Dapogny, and P. Jolivet, "Body-fitted topology optimization of 2D and 3D fluid-to-fluid heat exchangers," Comput. Methods Appl. Mech. Eng. **376**, 113638 (2021).
[20]J. K. Guest and J. H. Prévost, "Topology optimization of creeping fluid flows using a Darcy–Stokes finite element," Int. J. Numer. Methods Eng. **66**, 461–484 (2006).
[21]N. Barai and N. Mandal, "Breakup modes of fluid drops in confined shear flows," Phys. Fluids **28**, 073302 (2016).
[22]R. Dasgupta, J. Sen, and N. Mandal, "Bending curvatures of subducting plates: Old versus young slabs," Geophys. J. Int. **225**, 1981–2021 (1963).
[23]F. Okkels, M. Dufva, and H. Bruus, "Optimal homogenization of perfusion flows in microfluidic bio-reactors: A numerical study," PLoS One **6**, e14574 (2011).
[24]S. Shin, J. H. Jeong, D. K. Lim, and E. S. Kim, "Design of SFR fluidic diode axial port using topology optimization," Nucl. Eng. Des. **338**, 63–73 (2018).
[25]K. E. Jensen, "Topology optimization of stokes flow on dynamic meshes using simple optimizers," Comput. Fluids **174**, 66–77 (2018).
[26]J. Alexandersen, "A detailed introduction to density-based topology optimisation of fluid flow problems with implementation in MATLAB," Struct. Multidiscip. Optim. **66**, 12 (2023).
[27]C. Wu, C. Yang, Q. Xiao, H. Ke, and H. Xu, "Topology optimization of porous solid structures for heat transfer and flow channels in reactors with fluid-solid reaction coupling," Int. J. Therm. Sci. **181**, 107771 (2022).
[28]H. Tang, J. Zhu, Z. Tao, and L. Qiu, "Topology optimization with vortex-intensity-based objective function enables novel film cooling hole with superior performance," Phys. Fluids **36**, 085121 (2024).
[29]V. Pandey and P. S. Lee, "Fluid dynamic investigation of a topology-optimized liquid-cooled heat sink for enhanced performance," Phys. Fluids **37**, 033606 (2025).
[30]G. S. Beavers and D. D. Joseph, "Boundary conditions at a naturally permeable wall," J. Fluid Mech. **30**, 197–207 (1967).
[31]G. Neale and W. Nader, "Practical significance of Brinkman's extension of Darcy's law: Coupled parallel flows within a channel and a bounding porous medium," Can. J. Chem. Eng. **52**, 475–478 (1974).
[32]P. G. Saffman, "On the boundary condition at the surface of a porous medium," Stud. Appl. Math. **50**, 93–101 (1971).
[33]M. Hinze, R. Pinnau, M. Ulbrich, and S. Ulbrich, *Optimization with PDE Constraints* (Springer Science & Business Media, 2008), Vol. 23.
[34]K. Svanberg, "The method of moving asymptotes—A new method for structural optimization," Int. J. Numer. Methods Eng. **24**, 359–373 (1987).
[35]S. Kreissl, G. Pingen, and K. Maute, "Topology optimization for unsteady flow," Int. J. Numer. Methods Eng. **87**, 1229–1253 (2011).
[36]A. Evgrafov, "Topology optimization of slightly compressible fluids," Z. Angew. Math. Mech. **86**, 46–62 (2006).
[37]C. Y. Choi and P. M. Waller, "Momentum transport mechanism for water flow over porous media," J. Environ. Eng. **123**, 792–799 (1997).
[38]A. Goharzadeh, A. Khalili, and B. B. Jørgensen, "Transition layer thickness at a fluid-porous interface," Phys. Fluids **17**, 057102 (2005).
[39]GianmarcoBoscolo/FTOPT, see https://github.com/GianmarcoBoscolo/FTOPT for "Topology optimization code" (2024).